Journal of Inorganic and Organometallic Polymers and Materials (2023) 33:731–746
https://doi.org/10.1007/s10904-023-02532-z

RESEARCH

Preparation of Novel Composites of Polyvinyl Alcohol Containing Hesperidin Loaded ZnO Nanoparticles and Determination of Their Biological and Thermal Properties

Ibrahim Erol[1,4] · Ömer Hazman[1,3] · Mecit Aksu[2]

Received: 14 August 2022 / Accepted: 3 January 2023 / Published online: 19 January 2023
© The Author(s), under exclusive licence to Springer Science+Business Media, LLC, part of Springer Nature 2023

Abstract
Hesperidin (HSP) is considered to be the most effective antimicrobial agent against SARS-CoV2 virus. The HSP was loaded onto ZnO nanoparticles that were successfully incorporated, via the hydrothermal method, into polyvinyl alcohol (PVA) for use as food packaging material. The hydrothermal method enabled the bioactive ZnO-HSP to be homogeneously dispersed in the PVA, which significantly increased the thermal stability of the matrix, while decreasing the softening temperature. The water holding capacity and water solubility of the obtained nanocomposites was reduced compared to the PVA. Finally, the ZnO-HSP antimicrobial agent contributed important antibacterial properties to the PVA and increased its antioxidant capacity against *Staphylococcus aureus* and *Escherichia coli* pathogens. In addition, the nanocomposites had no cytotoxic/proliferative effects on cancer cells. All results showed promise that the PVA/ZnO-HSP nanocomposites would be an excellent alternative for food packaging applications.

Keywords PVA · ZnO · Hesperidin · Nanocomposites · Biological activity · Thermal properties

1 Introduction

Food packaging materials ensure that the products put in them are delivered to the consumer economically and reliably without spoilage. Plastics, one of the most frequently used materials in food packaging, are mainly produced from petroleum derivatives and are known to cause environmental pollution. For this reason, the production and use of synthetic and natural biopolymer-based biodegradable food packaging materials have recently gained importance. Biopolymers are naturally formed by biomass and can be decomposed by microorganisms in the environment. Therefore they are referred to as green polymers [1].

As one of the biodegradable polymers, polyvinyl alcohol (PVA) is a non-toxic, water-soluble, semi-crystalline synthetic biopolymer with excellent film-forming, emulsifying, and adhesive properties [2]. It has a wide range of uses in fields such as pharmacology, food chemistry, biomedicine, biotechnology, paper coatings, and the production of water-soluble flexible packaging films [3]. In recent studies, it has been reported that PVA is a safe material for food packaging because it is made from renewable resources and is environmentally friendly [4, 5].

According to the US Food and Drug Administration (FDA), zinc oxide nanoparticles (ZnO-NPs) are safe substances. Due to their low economic cost and low toxicity, ZnO-NPs are used as preservatives and packaging in the food industry [6]. They are widely used as drug carriers [7] and for cosmetics, food preservation, wound dressings [8], and medical filling materials due to their low cost and antibacterial activity. In addition to these features, the fact that ZnO-NPs have antiviral activity [9] suggests that they can be used in the development of useful products against the SARS-CoV2 virus.

✉ Ibrahim Erol
ierol@aku.edu.tr

1 Department of Chemistry, Faculty of Science and Arts, Afyon Kocatepe University, 03200 Afyonkarahisar, Turkey

2 Department of Chemistry, Faculty of Science and Arts, Düzce University, 81620 Düzce, Turkey

3 Department of Organic and Bioorganic Chemistry, Faculty of Chemistry, Samarkand State University, University bvld-15, Samarkand, Uzbekistan

4 Department of Polymer Chemistry and Chemical Technology, Faculty of Chemistry, Samarkand State University, University bvld-15, Samarkand, Uzbekistan

Many researchers have reported the antioxidant, anti-inflammatory, anti-allergic, and antimicrobial effects of HSP, an herbal pharmacological bioflavonoid [10, 11]. Data obtained from recent molecular docking studies show that hesperidin may have beneficial effects in the treatment of Covid-19 and the inactivation of the SARS-CoV2 virus [12, 13]. It is also stated that HSP can bind well to the spike proteins that mediate the binding of the virus to the ACE-2 receptor, thus preventing the virus from entering the cell [14, 15].

In this study, we first aimed to strengthen the ZnO-NPs with HSP and then to create strong antibacterial and antiviral effects by incorporating them into PVA via the hydrothermal method. The optical, thermal, mechanical, and antibacterial properties of the PVA-ZnO nanocomposites prepared by different methods have been investigated in recent studies in the literature [16, 17]. On the other hand, biodegradable films such as PVA have disadvantages such as poor mechanical strength and low gas exchange inhibition. It is thought that ZnO nanoparticles fortified with a plant-derived bioagent such as HSP would constitute an essential alternative option in food packaging applications due to their increased biocompatibility. The successful hydrothermal addition of ZnO-HSP nanoparticles to PVA results in the PVA's enhanced electrical, mechanical, and bioactive properties. Biodegradable nanocomposites containing the non-toxic PVA-ZnO-HSP can be used more effectively as environmentally friendly food packaging material. There is no information in the literature that nanocomposites containing HSP-loaded ZnO nanoparticles have been produced by hydrothermal method. The hydrothermal technique is an environmentally friendly and promises a good dispersion of nanoparticles in the matrix under high temperature and pressure in an aqueous medium. The ultimate aim of this study was to increase the quality and safety of packaging material through the ZnO-HSPs contained in the PVA.

2 Materials and Methods

2.1 Materials

The polyvinyl alcohol, zinc (II) acetate, sodium hydroxide, and hesperidin were purchased from Merck (Germany) and used without any purification. In addition, the following materials used in the study were obtained from the relevant companies: human malignant melanoma G-361 cells (ATCC), fetal bovine serum (Sigma), L-glutamine (Capricorn), penicillin-streptomycin (Thermo), RPMI 1640 (Sigma), total antioxidant assay kit (Elabscience), phosphate buffered saline (Sigma), dimethyl sulfoxide (Merck Millipore), and hesperidin (Cayman).

2.2 Preparation of ZnO Nanoparticles

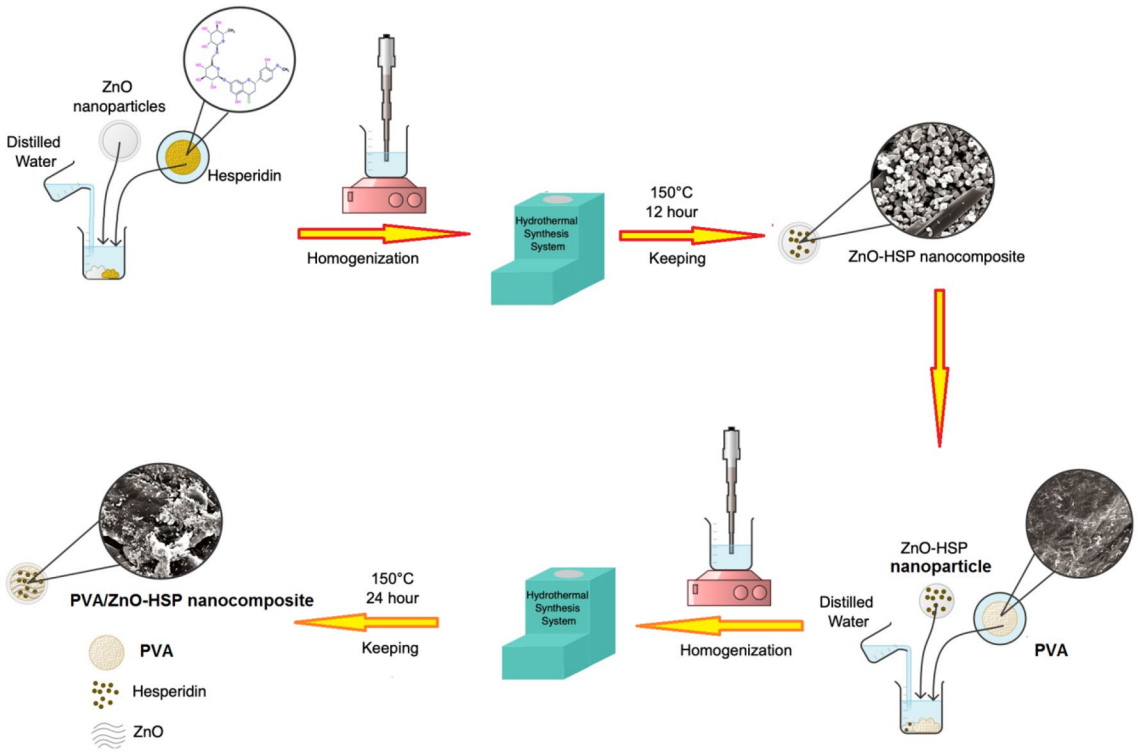
Zinc acetate dihydrate (0.1 M) solution was first put into a 50-mL beaker. This solution was then added dropwise to 0.2 M sodium hydroxide solution and dispersed for 20 min at 800 rpm with a magnetic stirrer. At the end of the period, the pH of the mixture was adjusted to 9 using a NaOH solution and then homogenized for about 10 min with an ultrasonic probe. The resulting mixture was transferred to a 100-mL Teflon container and kept in the hydrothermal synthesis system at 150 °C for 24 h. The ZnO particles formed at the end of the period were passed through filter paper, washed with distilled water, and dried in a vacuum oven at 60 °C for 8 h until they reached a constant weight.

2.3 Preparation of the ZnO-Hesperidin (ZnO-HSP)

In a 250-mL beaker, the ZnO nanoparticles (1 g) were added to 100 mg of the HSP and 100 mL of distilled water. The mixture was first homogenized with a magnetic stirrer at 600 rpm for 20 min and then with an ultrasonic probe for 20 min until it reached the appropriate consistency. Next, the mixture was transferred to a 100-mL Teflon container, placed in a hydrothermal synthesis device, and kept at 150 °C for 12 h. The resulting ZnO-HSP nanoparticles were filtered, washed with distilled water, and dried to constant weight in a vacuum oven at 70 °C for 10 h. In literature studies, similar active compounds have been successfully loaded to ZnO [18].

2.4 Preparation of the PVA/ZnO-Hesperidin (PVA/ZnO-HSP) Nanocomposites

The production of the PVA/ZnO-HSP nanocomposites was carried out via the hydrothermal method. The typical procedure for the preparation of nanocomposites containing 2% ZnO-HSP was followed. First, 1 g of the PVA was placed in a 50-mL beaker, to which 30 mL of distilled water was added. Next, 0.02 g of the ZnO-HSP was added to this mixture and mixed in a magnetic stirrer at 600 rpm for 30 min. Finally, the mixture, which was homogenized using an ultrasonic probe for 15 min, was transferred to a 100-mL Teflon container and placed in a hydrothermally operated nanomaterial production device and kept at 150 °C for 12 h. The composite obtained at the end of the period was filtered, washed with distilled water, and dried in a vacuum oven at 60 °C for 8 h. The same procedures were followed in preparing nanocomposites containing 4% and 6% ZnO-HSP. All production steps for the PVA/ZnO-HSP nanocomposites are shown in Scheme 1.



Scheme 1 Synthesis procedure for the PVA/ZnO-HSP nanocomposites

2.5 Characterization Techniques

Fourier-transform infrared (FTIR) spectroscopy (Shimadzu FT-IR Affinity 1 S, Japan) was used to determine the functional groups of the obtained nanocomposites. The FTIR spectra were recorded in the range of 400–4000 cm^{-1} using the KBr disc technique. Morphological analysis of the composites was performed by scanning electron microscopy (SEM) (NanoSEM 650, detector: TLC). The X-ray diffraction (XRD) analyses were recorded using a Bruker D8 Advance diffractometer with Cu K α radiation and a 2θ scanning speed at 1.281°/min and in the range of 20°–80°. Transmission electron microscopy (TEM) was used to determine the average size and distribution of ZnO nanoparticles in the nanocomposites. The TEM images were recorded using a Hitachi HT7800 transmission microscope at a voltage of 100 kV. The thermogravimetric (TG) properties and thermogravimetric analysis (TGA) of the composites were determined by the TG-60 and TGA-60 (Shimadzu, Japan) instruments. The differential scanning calorimetry (DSC) and TGA measurements were made in aluminum containers using 6–8 mg of substance in a nitrogen atmosphere.

2.6 Biological Properties of the PVA/ZnO-HSP Nanocomposites

2.6.1 Antibacterial Assay

Studies in the literature have shown that ZnO nanoparticles [19, 20], HSP [20–22], and PVA [16] exhibit antimicrobial activity. For these reasons, the antibacterial activities of the only synthesized nanocomposites were investigated in the present study. The results obtained were interpreted by comparing them with the antibacterial activities of the ZnO, HSP, and PVA mentioned in the literature.

The antibacterial activity of nanocomposites was determined by the disc diffusion method. For this, three 10-mm-diameter discs were created for each of the synthesized nanocomposites. The *Staphylococcus aureus* (ATCC 25,923) and *Escherichia coli* (ATCC 25,922) bacterial strains used in the study were enriched in peptone water. Suspensions were prepared at an average concentration of 10^6–10^7 CFU/mL by counting via the serial dilution method. Afterwards, incubation was carried out using 1 mL Petri dishes containing 25 mL Mueller-Hilton agar (Oxoid CM337). One day

later, the prepared nanocomposite discs and the antibiotic (moxifloxacin, Oxoid) disc used for the control were placed in Petri dishes and incubated for 24 h at 37 °C in an oven. At the end of the incubation, the zones of inhibition (mm) formed around each disc were measured [23].

2.6.2 Determination of Total Antioxidant Capacity

The total antioxidant capacity of the HSP, ZnO, ZnO-HSP, and nanocomposites was measured using a commercial kit (Elabscience, USA) as a trolox equivalent assay. The analyses were planned in triplicate. To compare the antioxidant efficiency of the materials used in the study, the trolox equivalent of the vitamin C used in the study was also measured. First, five separate (2; 1.5; 1; 0.5; 0.25 mmol Trolox/L) trolox standards were prepared. The absorbance values of the standards and samples were then determined at 660 nm (Biotek, Epoch) by following the kit protocol. The concentrations of the samples were calculated by using the absorbance of the calibration chart obtained. Because the trolox equivalent was used to express the antioxidant capacity, the results were expressed as mmol Trolox Equiv. /L.

2.6.3 Cytotoxicity Analysis

Studies conducted with both the SARS-CoV2 virus [24] and other viruses [25] indicate that HSP has cytotoxic effects against viruses and may be antiviral. Molecular docking studies have shown that hesperidin can inhibit the activity of SARS-CoV2 [15, 26]. It has also been reported that membranes produced with ZnO nanoparticles and PVA may exhibit protective effects against SARS-CoV2 [27]. For these reasons, the nanocomposites used in the present study were not investigated with SARS-CoV2 under in vitro conditions.

Human G-361 melanoma cells were used for cytotoxicity assays. During the study, the RPMI 1640 medium used contained 10% fetal bovine serum (FBS), 2 mM L-glutamine, 100 units/mL penicillin, and 100 µg/mL streptomycin. Cells were incubated in a sterile environment at 37 °C and 5% CO_2 in a CO_2 incubator (Thermo, Germany).

2.6.4 Preparation of Cells for Cytotoxicity Analysis

The G-361 melanoma cells were seeded in 75-cm^2 flasks containing ample medium. After sufficient proliferation, the cells were removed from the flask base using trypsin and then detrypsinized. Finally, the cell pellet collected at the bottom of a 15-mL falcon tube was suspended in 3 mL medium, and a cell count was performed using the trypan blue method [28]. The cytotoxicity levels of the synthesized PVA nanocomposites containing ZnO-HSP-NPs at different ratios in G-361 melanoma cells were determined by the MTT (3-4,5-dimethyl-thiazolyl-2,5 diphenyl tetrazolium bromide) method. The G-361 cells were seeded in a 96-well plate with 5,000 cells in 200 µL of the medium in each well. They were removed and placed in the incubator so that the cells adhered to the base of the flask and proliferated adequately. After incubation, the media of the cells were replaced with media containing nanocomposites at appropriate concentrations.

2.6.5 Preparation of Media Containing Nanocomposites Applied to Cells

Since the synthesized nanocomposites are not water-soluble, their cytotoxicity levels were determined using nanocomposite extracts obtained from incubating nanocomposites within the medium. For this, a 1:10 mixture of each nanocomposite and the medium was prepared. Next, 200 mg of each of the PVA nanocomposites containing the ZnO-HSP-NPs in different (2%, 4%, and 6%) ratios were weighed and put into a tube, and 2 mL of medium was added. The tube was sonicated in an ultrasonic water bath (Bandelin Sonopuls, Germany) for 30 min at 37 °C. The solution was then incubated in an oven at 37 °C for 24 h. At the end of the incubation, the media that interacted with the nanocomposites were put into separate tubes. Using the obtained nanocomposite extracts, media were prepared at four different concentrations, with dilution ratios of 1:1, 1:2, 1:4, 1:8 for each nanocomposite. The different dilutions of media with nanocomposites were applied to the cells before the MTT analysis and incubated for 24 h. To determine the effect of each prepared dilution on the cells, at least three repetitions were performed. The same volume of medium without nanocomposites was added to the control wells.

2.6.6 MTT Analysis

At the end of the incubation, 10% (20 µL) of each well volume was added to the 5 mg/mL concentration of the MTT solution prepared in a phosphate buffer (pH: 7.4). Cells were incubated for 3 h. At the end of the incubation, the medium in each well was carefully aspirated. Following this procedure, 200 µL of dimethyl sulfoxide (DMSO) was added to each well. The absorbance values of the solutions in each well were determined at 570 nm using a microplate reader (Biotek, Epoch). The cell viability of the control group, which was not treated with nanocomposites, was assumed to be 100%, and the effect of the media at different concentrations of each composite on cell viability was calculated using the equation given as (1) [29].

$$\text{Cell viability (\%)} = \left[\left(100 \times \text{Absorbance}_{\text{sample}}\right) / \left(\text{Absorbance}_{\text{control}}\right) \right] \quad (1)$$

2.7 Determination of Thermal Degradation Kinetics of the PVA/ZnO-HSP

The effect of the ZnO-HSP nanoparticles on the thermal stability of the pure PVA was determined by the non-isothermal kinetic Kissinger-Akahira-Sunose (KAS) analysis method [30]. The thermal decomposition activation energy (E_a) values of the nanocomposites were determined from the thermograms obtained at different heating rates (5, 10, 15, and 20 °C min^{-1}). The KAS method is based on taking the differential of Eq. (2).

According to this,

$$\ln\left(\frac{\beta}{T^2}\right) = \ln\left(-\frac{AR}{E_a \ln(1-\alpha)}\right) - \frac{E_a}{R\,T} \tag{2}$$

where β is the heating rate, T is the temperature, and R is the ideal gas constant; ln (β/T^2) against (1/T) gives the activation energy from the slope.

2.8 Determination of Water Solubility rate

The effect of the ZnO-HSP on the water solubility of the pure PVA was determined using the method presented in the literature [31]. All samples were kept in a thermostated oven at 110 °C to remove moisture until they reached constant weight.

The samples taken from the oven were then placed in a beaker containing 50 mL of water and mixed at 400 rpm using a magnetic stirrer for 8 h. At the end of the period, the samples were taken out of the beaker, at first kept in the open air, and then in a thermostated oven at 110° C. Once they had reached a constant weight, they were weighed. The % water solubility ratio was determined using the following equation;

$$\text{Water solubility} = W_1 - W_2/W_1 \times 100 \tag{3}$$

where W_1 is the weight before the films are put into water, and W_2 is the weight after waiting.

2.9 Swelling Study

One of the important parameters taken into account in determining the biocompatibility of a material and deciding whether it can be used for biomedical purposes is its water-holding capacity. The gravimetric method was used to determine the swelling behavior of the PVA and nanocomposites. Samples at certain weights were immersed in pH 7.4 phosphate buffer solution, and after 48 h, excess water on the surface of the films was removed with filter paper, and they were weighed again. Swelling properties of the samples were determined by using Eq. (4).

$$\text{Swelling rate (\%)} = \left(W_t - W_0/W_0\right) \times 100 \tag{4}$$

where W_0 is the dry weight of the product and W_t is its weight at the end of 48 h. All swelling experiments were repeated three times.

2.10 Statistical Analysis

The cytotoxicity, antibacterial, and antioxidant capacity analyses were performed with at least three replications, and thus, the data obtained were defined as mean ± standard deviation. The SPSS 20 package program was used to evaluate the data statistically. Statistical differences between data were detected using one-way analysis of variance (ANOVA) and Duncan's post-test.

3 Results and Discussion

3.1 Interaction Mechanism Between the PVA and the ZnO-HSP

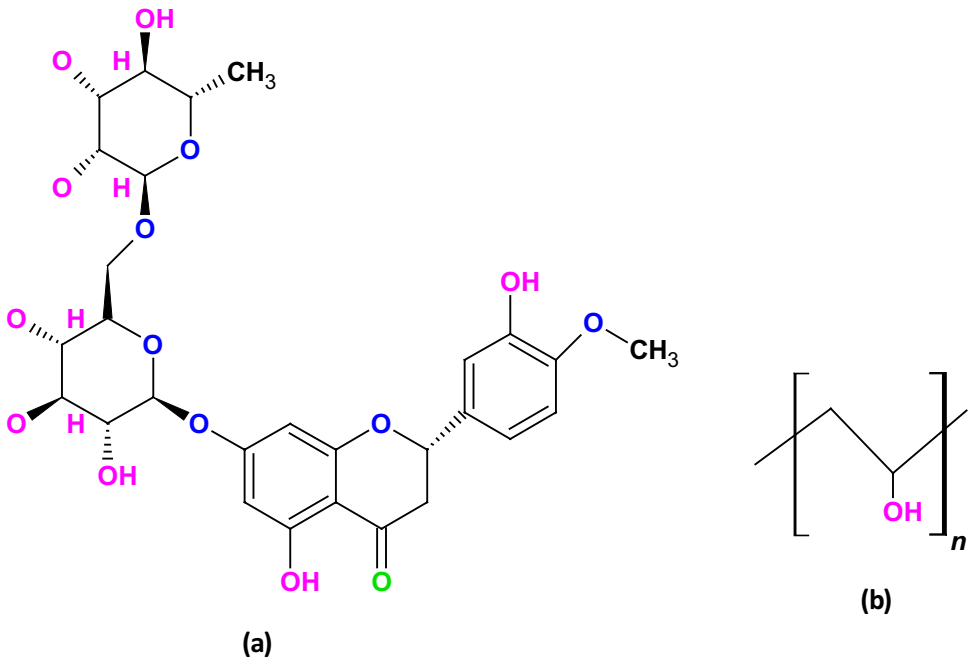
The chemical structure of the HSP and the PVA is shown in Scheme 2.

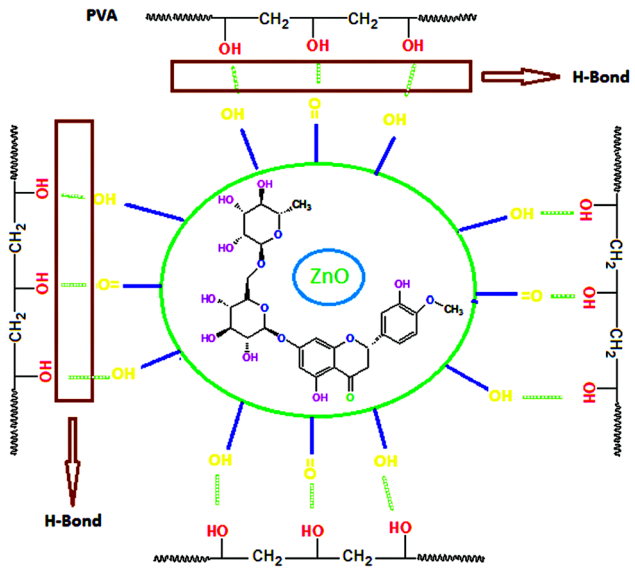
As seen in Scheme 3, in the hydrothermal system, between the hydroxyl groups in the side branch of the PVA and the multiple hydroxyl and carbonyl groups in the molecular structure of the HSP, intermolecular hydrogen bonds are formed between the electronegative oxygen atoms and the less electronegative hydrogen atoms. In addition, the ZnO nanoparticles in the environment can form hydrogen bonds with the OH and carbonyl groups of the HSP and the PVA due to the presence of moisture adsorbed on the surface as well as from the oxygen atom. Such interactions between the three components lead to a cross-linked network-type structure. This structure is responsible for the physicochemical, thermal, and biological properties of the nanocomposites examined in this study.

3.2 FTIR Analyses

The FTIR spectra of the pure PVA, ZnO-HSP, and nanocomposites are shown in Fig. 1. One of the characteristic peaks in the FTIR spectrum of the pure PVA is the OH stretching vibration bands seen at 3475 cm^{-1}. As a result of the hydrolysis of the PVA, the peaks seen at 1652 cm^{-1} are due to residual acetate groups [32]. Another important signal in the FTIR spectrum of the PVA is due to the O–H bending vibrational bands, which peak at 1636 cm^{-1} [33]. The bending and wagging vibrational bands of the aliphatic

Scheme 2 Chemical Structure of **a** the HSP and **b** the PVA





Scheme 3 H bonding formation between the PVA and the ZnO-HSP

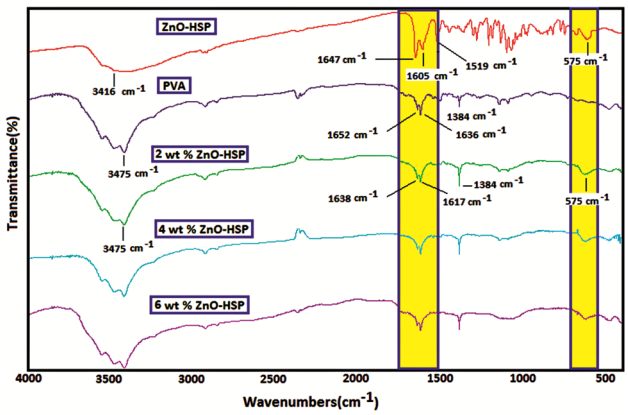


Fig. 1 The FTIR spectum of HSP, ZnO-HSP,CS and nanocomposites

CH_2 groups of the PVA give signals at 1384 and 1425 cm^{-1}, respectively. The C-O stretching vibration bands originating from the C and OH groups in the main chain were observed at 1252 cm^{-1} [33]. The broadband observed at 3500 cm^{-1} in the FTIR spectrum of the ZnO-HSP nanoparticles was attributed to the stretching vibrations of the OH groups present in the structure of the HSP and on the surface of ZnO. The peak observed at 1647 cm^{-1} belongs to the C=O stretching vibration bands of the HSP. The ArC=C stretching vibrations gave a moderate intensity peak at 1605 cm^{-1}. The presence of the Zn–O bond in the FTIR spectrum of the ZnO-HSP was determined by the signal appearing at 575 cm^{-1} [34].

The FTIR spectra of the PVA/ZnO-HSP nanocomposites differed from the pure PVA. In particular, the peaks observed at 1650–1620 cm^{-1} for pure PVA and the ZnO-HSP differed, with new peaks signaling at 1638 and 1717 cm^{-1}. The possible reason for this situation is the interactions between the C=O and OH groups of the ZnO-HSP and the OH groups of the PVA [35]. In addition, Zn–O stretching vibration bands were observed in the nanocomposites at 575 cm^{-1}, and their intensity slightly increased with the ZnO concentration.

As seen in Scheme 2, in the hydrothermal system, between the hydroxyl groups in the side branch of the PVA and the multiple hydroxyl and carbonyl groups in the

molecular structure of the HSP, intermolecular hydrogen bonds are formed between the electronegative oxygen atoms and the less electronegative hydrogen atoms. In addition, the ZnO nanoparticles in the environment can form hydrogen bonds with the OH and carbonyl groups of the HSP and the PVA due to the presence of moisture adsorbed on the surface and from the oxygen atom. Such interactions between the three components lead to a cross-linked network-type structure.

3.3 XRD Analysis

In Fig. 2, the X-ray diffraction patterns of ZnO, ZnO-HSP, PVA, and nanocomposites in the 2θ = 20°–80 are shown. XRD model of ZnO, at 2θ = 31.80° (100), at 2θ = 34.51° (002), at 2θ = 36.41 (101), at 2θ = 47.63° (102), at 2θ = 56.43° (110), at 2θ = 61.76° (103) and at 2θ = 69.83° (112) showed characteristic peaks at corresponding planes. The strong and sharp diffraction peaks observed indicate that highly crystalline ZnO nanoparticles are formed, and the tightly packed hexagonal Wurtzite structure agrees with the reported JCPDS (36-1451) data [36] No significant change in XRD patterns was observed after surface modification of the ZnO nanoparticles with the HSP. The sharp and broad peaks around 2θ = 19.23° and 40.15°, corresponding to the crystal area and semi-crystalline nature of the pure PVA, indicate that the PVA contains a large amount of crystal area [37]. With the addition of the ZnO-HSP to the PVA matrix, characteristic diffraction patterns of the ZnO appeared as well as the peak at 2θ = 19.23° of the amorphous PVA. These reflections confirm the presence of the ZnO-HSP nanoparticles in the PVA. In addition, the intensity of the peaks in the XRD patterns of the nanoparticles, especially at 2θ = 31.80, 34.51, and 36.41, increased significantly with the concentration of the ZnO-HSP. The crystal size of the ZnO nanoparticle was evaluated by measuring the FWHM of the most intense peak (101), as it has a relatively strong intensity and does not overlap with other diffraction peaks. As seen in Fig. 3, the crystal size of the ZnO nanoparticles was found to be about 46 nm. The results show the physical compatibility of the ZnO-HSP with the PVA matrix in nanocomposite systems prepared by the hydrothermal method.

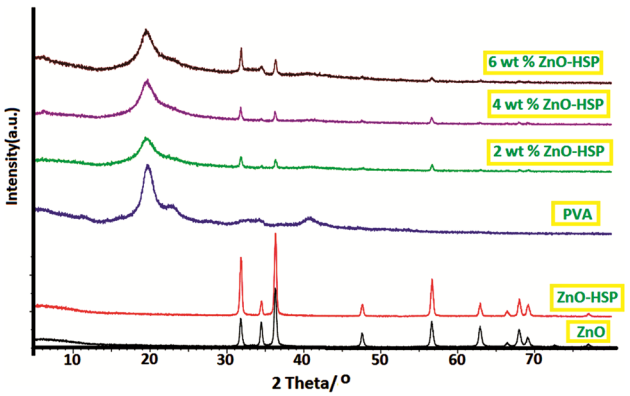


Fig. 2 XRD pattern of PVA, ZnO, ZnO-HSP and nanocomposites

3.4 SEM, TEM, and EDX Analyses

The distribution state, surface morphology, and physical interactions of the ZnO-HSP nanoparticles in the PVA matrix were investigated using SEM (Fig. 4). The SEM image in Fig. 5a shows that the pure PVA has a mostly smooth surface. The SEM image of the ZnO nanoparticles

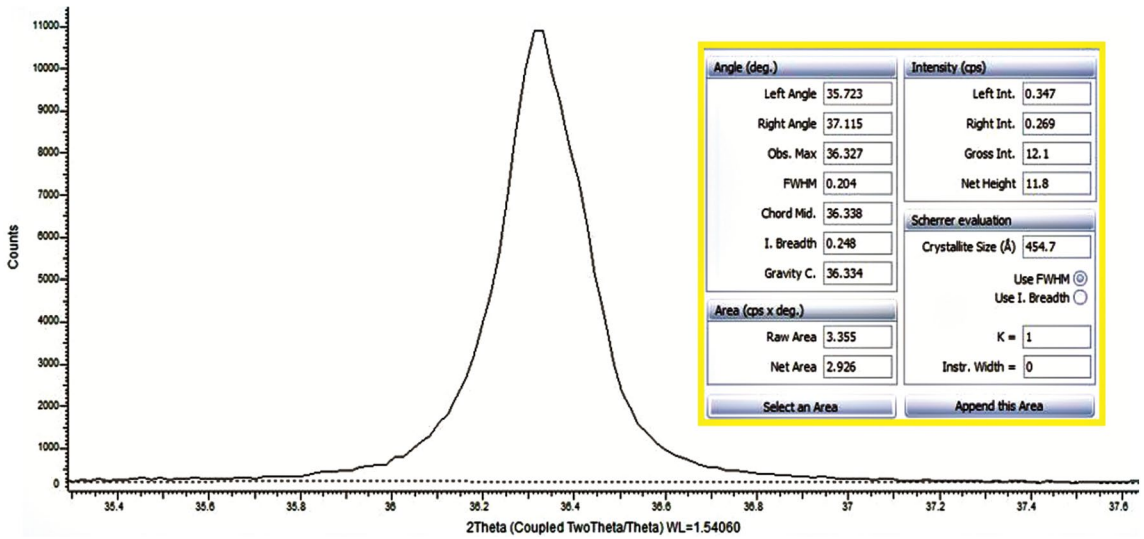


Fig. 3 The crystal size at the peak 36.25° of ZnO nanoparticles

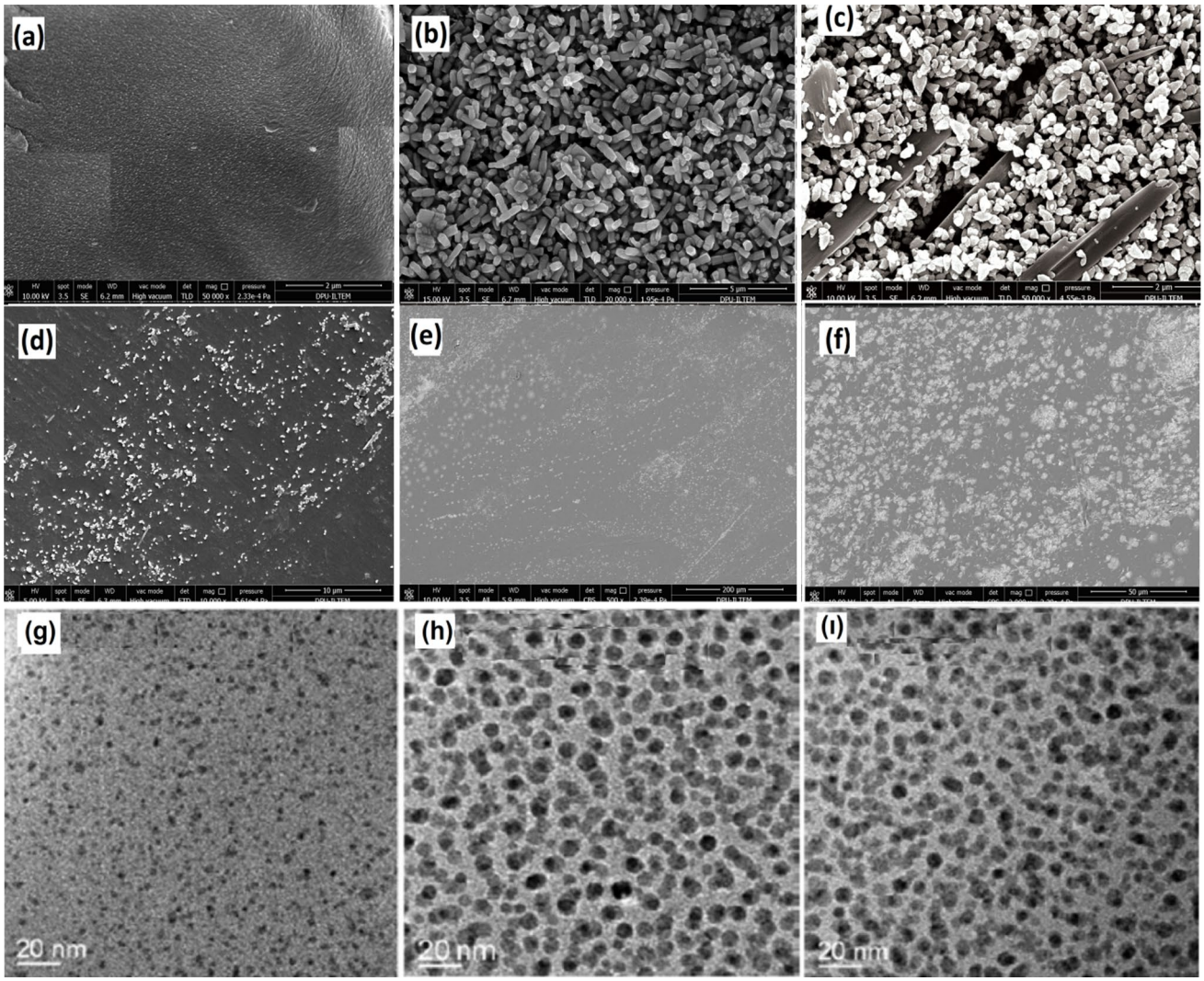


Fig. 4 SEM images of **a** PVA, **b** ZnO, **c** ZnO-HSP, **d** 2 wt% ZnO-HSP, **e** 4 wt % ZnO-HSP, **f** 6 wt% ZnO-HSP, TEM images of **g** 2 wt% ZnO-HSP, **h**) 4 wt % ZnO-HSP (ı)) 6 wt % ZnO-HSP.

seen in Fig. 4b changed significantly when the HSP was added, and the HSP molecules became visible, as seen in Fig. 4c. An effective physical interaction occurred between the two molecules because of the hydrogen bonds between the OH groups on the surface of the ZnO and the OH and C=O groups on the HSP molecule.

As seen in Fig. 4d–f, with the addition of the ZnO-HSP at different rates to the PVA, the nanoparticles generally showed a homogeneous distribution on the matrix surface. However, partial aggregation was observed in some regions in the nanocomposite containing 6% ZnO-HSP (Fig. 4f). The reason for this situation was the increase in surface energy with the amount of ZnO [38]. In contrast, the reason for the homogeneous distribution at low ZnO-HSP ratios was the increase in the surface stabilization provided by the hydrogen bonds between the OH groups of the PVA and the OH and C=O groups of the ZnO-HSP [30]. The homogeneous distribution of the ZnO-HSP filler in the PVA matrices resulted in good affinity, high thermal stability, and superior biological activity [38].

The TEM images of the nanocomposites in Fig. 6 provide information on the particle size and distribution of the ZnO nanoparticles in the nanocomposite. The micrographs confirmed that the ZnO nanoparticles in all three nanocomposites were nano-sized and quite well dispersed in the PVA matrix.

The EDX analysis was performed to investigate the elemental composition of the nanocomposites. The EDX spectrum of the nanocomposite containing 6% by mass of the ZnO-HSP is presented in Fig. 5. Three elements emerged, i.e., carbon, zinc, and oxygen, resulting from the carbon backbone of the PVA and the ZnO-HSP content

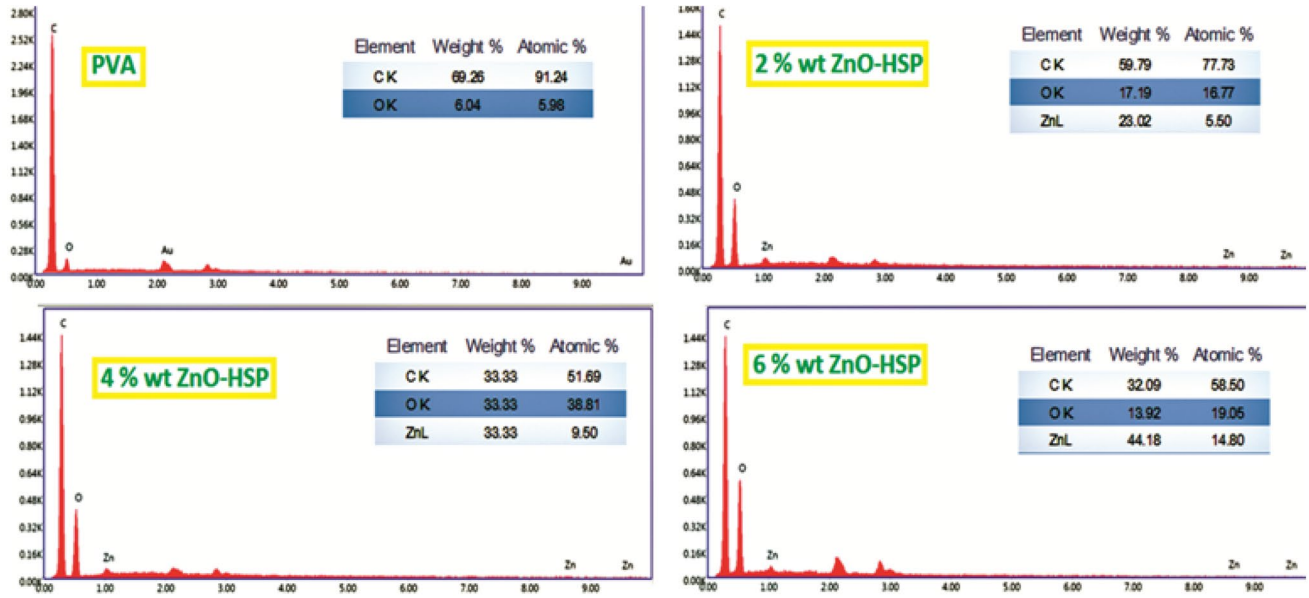


Fig. 5 EDX analysis of the PVA and nanocomposites

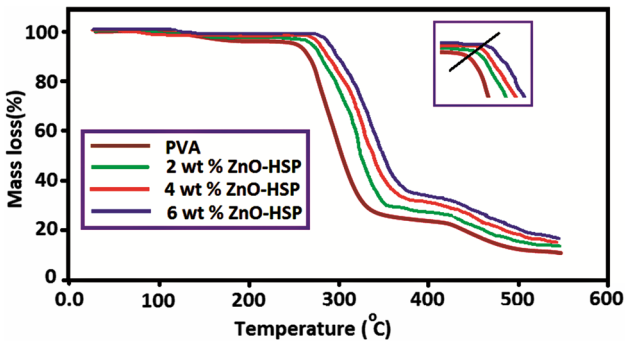


Fig. 6 TGA graph of the PVA and nanocomposites

Table 1 TGA measurement results of the pure PVA and PVA/ZnO-HSP nanocomposites

Sample	T_g (°C)[a]	T_i (°C)[b]	$T_{\%50}$ (°C)	Residue at 600 °C (%)
PVA	68	250	300	6
2 wt % ZnO-HSP	76	265	316	8
4 wt % ZnO-HSP	84	274	321	10
6 wt % ZnO-HSP	93	285	344	13

[a] T_g: glass transition temperature

[b] T_i: initial decomposition temperature

of the samples. The spectra showed that the zinc content increased with the increasing ZnO-HSP concentrations in the PVA matrix.

3.5 TGA Analysis

The effect of the ZnO-HSP nanoparticles on the thermal stability of the pure PVA was investigated by the TGA method. The thermograms presented in Fig. 6 were obtained at a heating rate of 20 °C/min in an inert nitrogen atmosphere. Some important data obtained from the thermograms are shown in Table 1. The thermal degradation of pure PVA took place in three different steps, as stated in the literature [39].

The second decomposition step of the PVA occurred around 250–360 °C, and chain-scission and cyclization reactions dominated in this step due to the degradation of the side chain. In addition, this step involved the continuous elimination of residual acetate groups. At this stage, the total weight loss had reached approximately 69% by weight [39].

The third stage occurred at 405–510 °C and may have resulted from the breakdown of large polymer chains into small volatile products that underwent further decomposition. The residual amount left by the PVA at 600 °C was about 4% [40].

The PVA/ZnO-HSP nanocomposites were also involved in three different thermal decomposition steps. However, the initial decomposition temperatures were considerably higher than that of the PVA. Although the nanocomposite containing 2% ZnO-HSP started to decompose at 265 °C, the same value reached 285 °C with an increase of 20 °C for the nanocomposite containing 6% ZnO-HSP. The main reason for this result was the strong hydrogen bond formation between the OH groups in the side branch of the PVA and

the OH and C=O groups in the ZnO and the HSP. The same phenomenon has been reported in previous studies [41].

The results also show that the ZnO-HSP nanoparticles added to the pure PVA delayed thermal degradation by forming a barrier for the volatile products released because of thermal degradation [42]. Another significant finding in the thermograms of the nanocomposites was the amount of residue at 600 °C. Table 1 shows that as the concentration of the ZnO-HSP in the PVA increased, the amount of residue resulting from degradation also increased. This result was related to the thermal stability of the ZnO nanoparticles at 600 C. In Fig. 6, the results show that the ZnO-HSP filler improved the thermal stability of the PVA.

3.6 DSC Analyses

The glass transition temperatures of the PVA and nanocomposites were determined from the DSC curves shown in Fig. 7, and the obtained values are shown in Table 1. The resulting T_g of the PVA was 68 °C. The T_g value of the pure PVA increased with the addition of the ZnO-HSP. The T_g value of the nanocomposite containing 2% by weight of ZnO was 76 °C, whereas this value increased to 93 °C for the composite containing 6% by weight of the ZnO-HSP.

This result shows that the ZnO-HSP filler dispersed in the amorphous PVA limited the chain mobility of the polymer molecules, causing a decrease in free volume and an increase in the T_g value. In addition, another reason for the rise in the T_g values of the nanocomposites was the hydrogen bonds formed between the OH groups of the PVA and the OH and C=O polar groups carried by the ZnO-HSPs. Scheme 2 shows possible H bonds formed between the PVA and the ZnO-HSP nanoparticles. It has been reported in the literature that nano-metal oxides added to polymer matrices cause a significant increase in T_g values [43]. The DSC data showed that the softening temperature of the pure PVA had been significantly increased because of the ZnO-HSP fillers. This result indicates the advantage of using PVA as a food packaging material, especially in high-temperature environments.

3.7 Thermal Kinetic Studies

The parameters of the KAS method were determined with the data obtained from the thermograms of the pure PVA and nanocomposites at different heating rates. The thermal decomposition activation energy (E_a) values in Table 2 were estimated by plotting $\ln\beta/T^2$ -1000/T graphs for each material. As seen in Fig. 8, parallel lines were obtained when the results of the KAS analysis of the 4 wt% ZnO-HSP nanocomposite were plotted. The E_a values calculated at different conversion intervals (α) for the pure PVA and nanocomposites are shown in Table 2. The calculated mean

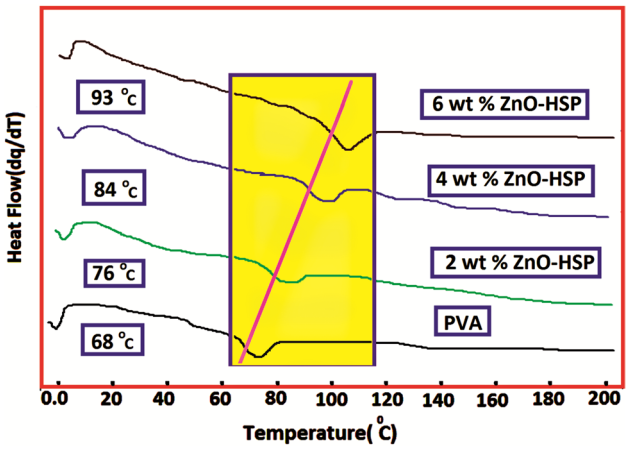


Fig. 7 DSC curves of the PVA and nanocomposites

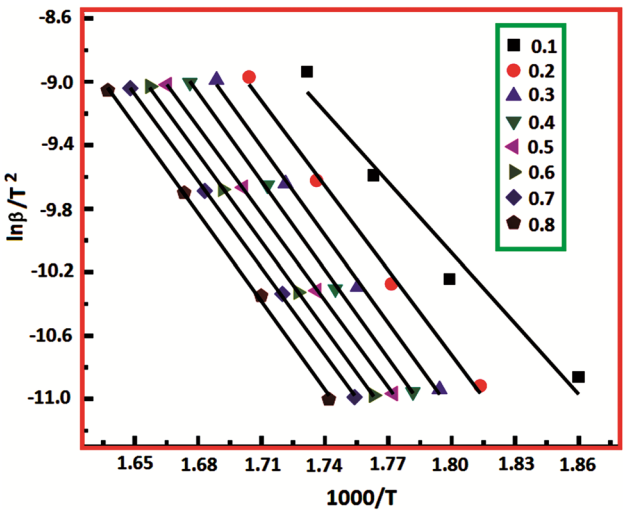


Fig. 8 KAS plot of 4 wt % ZnO-HSP nanocomposite

Table 2 Apparent activation energy values by KAS method of PVA and nanocomposites

Sample	Activation energy (kJ/mol) at conversion (α)								
	0.1	0.2	0.3	0.4	0.5	0.6	0.7	0.8	Aver.
PVA	44	55	148	153	161	170	213	224	146
2 wt % ZnO-HSP	55	63	151	159	167	182	221	234	154
4 wt % ZnO-HSP	62	69	166	177	192	198	228	238	166
6 wt % ZnO-HSP	73	80	174	185	196	205	238	244	174

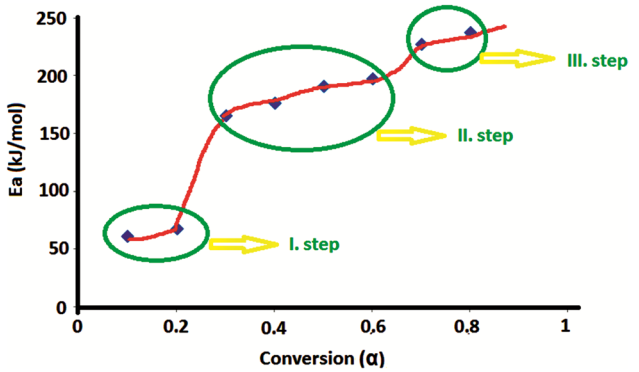


Fig. 9 The Ea values at the different conversion of the 4% ZnO-HSP nanocomposite

E_a of the PVA was 153 kJ/mol. The E_a values of the polymer nanocomposites containing 2, 4, and 6% by weight ZnO were 158, 175, and 187 kJ/mol, respectively. The results in Table 2 showed that the E_a values increased with the increase in the amount of the ZnO-HSP in the nanocomposites. This finding demonstrates that the ZnO-HSP NPs increased the thermal stability of the PVA.

Figure 9 shows the E_a values corresponding to different conversion values of the nanocomposite containing 4% ZnO-HSP. The average E_a value calculated in the transformation interval ($\alpha = 0.1–0.2$) corresponding to the 1st thermal decomposition step in which the water on the surface of the nanocomposite evaporates was found to be 66 kJ/mol. In the second degradation step, corresponding to the main chain break, the average E_a value calculated for the 03-0.6 transformation interval was 183 kJ/mol, and for the final degradation step corresponding to the 0.6–0.8 transformation interval, where volatile products are formed, the calculated average E_a value was 233 kJ/mol. Similar results were obtained for the other nanocomposites.

A significant increase was observed when the present results were compared with the E_a values of PVA-ZnO nanocomposites in the literature, prepared by the solution casting method and containing ZnO without the HSP loading [38]. This increase may be attributed to the hydrothermal method and the HSP used in the preparation of the nanocomposites. The high temperature and pressure effect in the hydrothermal method contributed to the homogeneous distribution of the ZnO nanoparticles and their physical interaction with the matrix. On the other hand, because of its functional groups, the HSP facilitated interaction with the matrix, we have obtained similar results in our recent studies [44, 45].

3.8 Determination of Antibacterial Activity

Escherichia coli was used as a Gram-negative bacteria strain and *S. aureus* was as a Gram-positive bacteria strain to determine the antibacterial activity of the PVA

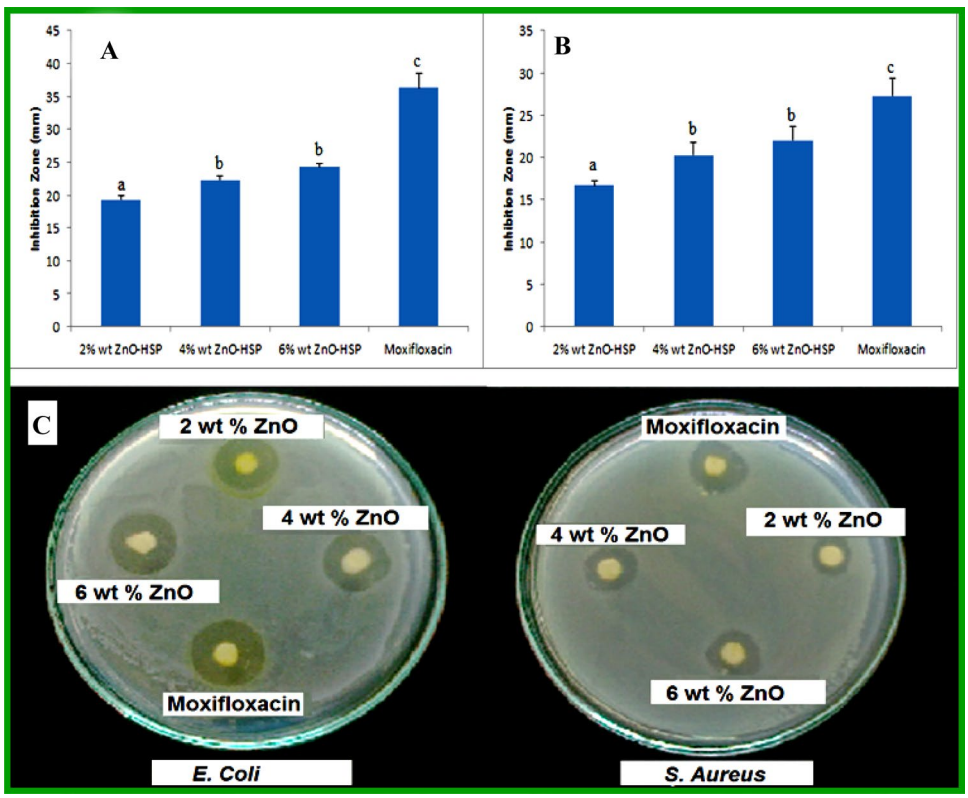


Fig. 10 Antibacterial activty results and image of nanocomposites (**A** *E.coli*; **B** *S.aureus*)

and nanocomposites. The antibacterial activity results obtained using discs made of nanocomposites and the antibiotic (moxifloxacin) disc used as control are presented in Fig. 10. The antibacterial effect of nanoparticles is the result of the reactive oxygen species (ROS) they form on their surfaces. The ROS can perform the lipid peroxidation reaction that disrupts the cell membrane structure by first partially rupturing the outer membrane of the bacterial cell, and then passing through the cytoplasmic membrane, causing the cell to die [46]. In the study, it was accepted that the PVA had no antibacterial effect [16]. As seen in Fig. 10 A and B, the average inhibition zones formed by the nanocomposites in the Petri dishes showed antibacterial properties against both *E. coli* and *S. aureus* bacterial strains. It was observed that the antibacterial effect increased dose-dependent as the ZnO-HSP concentration in the nanocomposites was increased. Figure 10 A clearly shows that the nanocomposites were more effective against the *E. coli* pathogen. This is likely because the cell wall of Gram-negative bacteria has a thin layer of peptidoglycan. An image of the zones formed by the nanocomposites against microorganisms after incubation is presented in Fig. 10 C. According to the results, the PVA matrix gained remarkable biological activity because of the ZnO-HSP bioagent. This indicates that the PVA is a safer biomaterial for food packaging.

3.9 Determination of Antioxidant Activity

The antioxidant capacity status of the nanocomposites was compared with that of vitamin C (Table 3). The antioxidant capacity of HSP was determined to be close to that of vitamin C.

As seen in Fig. 11 A, the antioxidant levels of the ZnO nanoparticles were very low. However, when the ZnO nanoparticles were loaded with the HSP, they exhibited antioxidant activity. They could carry these properties to the PVA-based nanocomposites into which they were added at different rates. It was observed that the antioxidant capacities

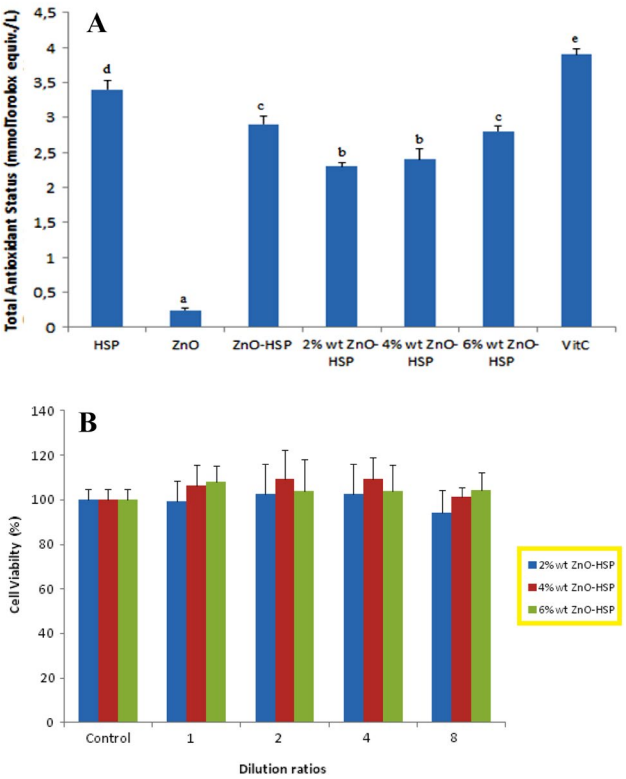


Fig. 11 **a** Antioxidant activity of HSP, ZnO, ZnO-HSP and nanocomposites. Data were given as mean ± standard deviation (n = 3). Statistical differences between data are given in superscript (a, b, c, d, e). Data without the same superscript differ from each other statistically ($p < 0.05$). **b** Cytotoxicity level of the nanocomposites. Data were given as mean ± standard deviation (n = 3)

Table 3 Antioxidant activity of HSP, ZnO, ZnO-HSP, vitamin C, and nanocomposites

Sample	Total antioxidant status (mmol Trolox Equiv./L)
HSP	3.40 ± 0.12^{d}
ZnO	0.24 ± 0.03^{a}
ZnO-HSP	2.88 ± 0.15^{c}
2 wt % ZnO-HSP	2.33 ± 0.05^{b}
4 wt % ZnO-HSP	2.38 ± 0.16^{b}
6 wt % ZnO-HSP	2.76 ± 0.07^{c}
Vitamin C	3.90 ± 0.08^{e}
P-value	0.000

Data were given as mean ± standard deviation (n = 3). Statistical differences between data are given in superscript ($^{a, b, c, d, e}$). Data without the same superscript differ from each other statistically ($p < 0.05$)

Table 4 Effect of nanocomposites on cell viability in G-361 melanoma cells

Dilution ratios	Nanocomposite extracts applied to cells		
	2 wt% ZnO-HSP	4 wt% ZnO-HSP	6 wt% ZnO-HSP
Control	99.97 ± 4.78	99.97 ± 4.78	99.97 ± 4.78
1:1	99.35 ± 9.06	106.51 ± 9.22	112.45 ± 7.15
1:2	102.61 ± 13.46	109.46 ± 12.73	103.95 ± 14.11
1:4	102.70 ± 13.51	101.34 ± 9.50	104.49 ± 11.77
1:8	94.13 ± 10.33	102.42 ± 4.11	104.50 ± 7.84
P-value*	0.790	0.532	0.504

Data were given as mean ± standard deviation (n = 3)

*It was determined that PVA nanocomposites containing different ratios of ZnO-HSP had no statistical cytotoxic/proliferative effect ($p < 0.05$) in human G-361 melanoma cells

of the nanocomposites increased in direct proportion to the increase in the ZnO-HSP ratios used.

The results showed that the nanocomposites gained effectiveness in providing detoxification by preventing the formation of ROS and their damage due to the ZnO-HSP NPs. Because of this feature, the PVA nanocomposites were able to react with the radicals very quickly and prevent the progression of auto-oxidation/peroxidation. Thus, they could contribute to the prevention of diseases by neutralizing excess free radicals and protecting cells against their toxic effects.

As seen in Table 3, the antioxidant effect of the ZnO nanoparticles was negligible. Moreover, it has been reported that ZnO nanoparticles may show pro-oxidant effects by increasing the formation of ROS rather than their antioxidant properties [13, 47]. However, it was determined that when loaded with ZnO, the HSP gained antioxidant properties (Fig. 11; Table 4). This antioxidant activity may be associated with the high antioxidant capacity of the HSP [48, 49]. Therefore, in the present study, the PVA-based nanocomposites containing the ZnO-HSP in different proportions were strengthened by the HSP.

The fact that the ZnO-HSP nanoparticles increased the antioxidant capacity of the PVA means that these nanocomposites can inhibit the growth of pathogenic microorganisms on the surface resulting from food contamination or large areas of fungal spoilage.

3.10 Determination of Cytotoxicity Activity

As seen in Table 4, it was determined that the extracts obtained from the PVA nanocomposites containing the ZnO-HSP did not statistically affect cell viability when applied to human G-361 melanoma cells, i.e., the synthesized nanocomposites were not cytotoxic.

It was determined that the ZnO-HSP-PVA nanocomposites produced by the presented study showed antibacterial activity in human G-361 melanoma cells without causing any proliferation or cytotoxicity. The antibacterial activity was probably due to the ZnO nanoparticles introduced together with the HSP into the nanocomposites because it has been stated in different studies [19, 50] that ZnO nanoparticles can exhibit antibacterial activity even at low concentrations. The cytotoxic activity of the ZnO against bacteria was not seen in the human cells, which may be related to the fact that low doses of ZnO are not cytotoxic to human cells.

Thus, in another work using ZnO-NPs on the A375 melanoma cell line, it was determined that the ZnO-NPs were not cytotoxic at low doses (5 µg/mL) on the melanoma cells [51]. In the present study, when ZnO-HPS was added to the PVA, it was calculated that even a high concentration of ZnO (6%) had a low probability of affecting the cells. It could be deduced that the ZnO-HSP-PVA nanocomposites were not cytotoxic because the concentration did not reach the cytotoxic limit value (5 µg/mL) mentioned in the literature, even at the highest dilution ratio of 1:1, where all the ZnO in the nanocomposite was accepted as digested by the extract (3 µg/mL). The goal was to achieve antibacterial effectiveness for the PVA-based nanocomposite via the ZnO-NPs and the antiviral efficacy of the HSP. Prior studies have indicated that low doses of HSP are not cytotoxic/proliferative on cancer cells [52] or healthy human cells [53].

It has been reported in the literature that PVA-ZnO nanocomposites showed antimicrobial activities and were effective against SARS-CoV2 [27, 54]. In the present study, a new nanocomposite was developed by using HSP together with PVA-ZnO. Experimental studies have shown that HSP has inhibitory properties against SARS-CoV2 [24]. For this reason, it was thought that the nanocomposites developed using HSP and PVA-ZnO in the present study might exhibit antiviral activity and antimicrobial properties.

Consequently, nanocomposites produced with the HSP-loaded ZnO particles could be added to the structure of various materials to prevent bacterial and viral contamination. Moreover, nanoparticles containing HSP could be used in producing useful materials by including natural or synthetic (such as PVA) polymers to reduce the transmission of COVID-19.

Figure 11B shows that the PVA/ZnO-HSP nanocomposites were not cytotoxic, even at high doses. Considering that the ZnO-HSP nanoparticles added to the PVA were not cytotoxic, the synthesized nanocomposites did not show cytotoxic effects. The addition of the ZnO-HSP reduced the cytotoxicity of the PVA. Therefore, these nanocomposites could be used in various advanced biomedical applications such as wound dressing, drug delivery systems and artificial organs. Depending on their use in various materials, the PVA/ZnO-HSP nanocomposites produced in the present study could be rapidly metabolized and should not show any toxic effects when taken into the body. It has been reported that, since no degradation products were detected in urine and feces, PVA is thus very stable in the body and can be metabolized rapidly [55, 56]. The ZnO, as the second principal component of the PVA/ZnO-HSP nanocomposites used in the study, may have beneficial effects in terms of metabolism because Zn is one of the trace elements of metabolic importance. Zinc oxide nanoparticles (ZnO-NPs) stand out among the Zn compounds. These ZnO-NPs can be produced rapidly by various synthesis processes and can be absorbed by the body faster than Zn alone. Due to their low economic cost and toxicity, ZnO-NPs are used as preservatives and in packaging by the food industry [6]. In addition to these properties, the fact that ZnO-NPs have antiviral activity [9] suggests that they could be used to develop valuable products against the SARS-CoV2 virus. It is known that HSP, the

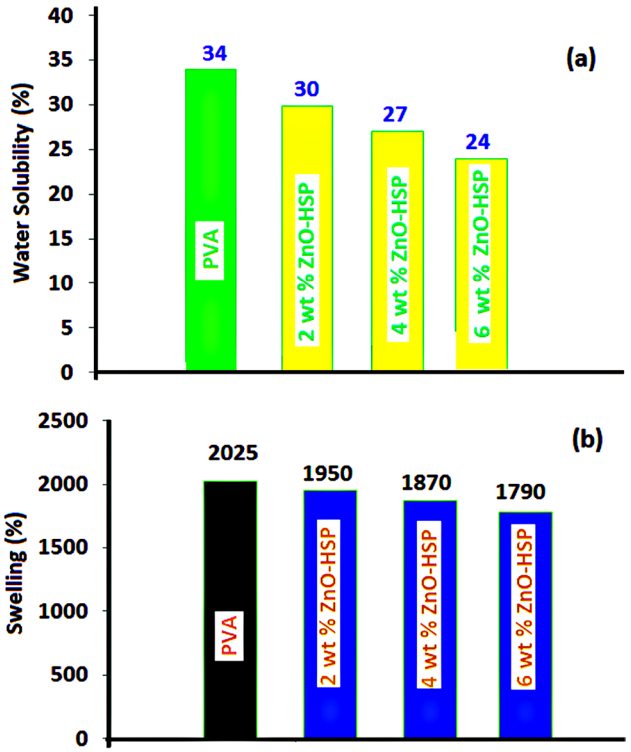


Fig. 12 **a** Water solubility and **b** swelling (%) value of pure PVA and nanocomposites

third component of the PVA/ZnO-HSP nanocomposite used in the study, exhibits vigorous antioxidant activity [48, 49, 57]. Therefore, the present study demonstrated that PVA-based nanocomposites containing ZnO-HSP at different rates had gained antioxidant activity through HSP. In light of this information, PVA/ZnO-HSP nanocomposite has the potential to be used safely in food packaging.

3.11 Water Solubility Testing

The effect of the ZnO-HSP NPs on the water solubility of the PVA was investigated via a water solubility test, and the results are presented in Fig. 12a. The solubility value of pure PVA in water reached 34% after 8 h.

With the addition of the ZnO-HSP nanoparticles to the PVA, the solubility value of the PVA in water decreased. The nanocomposites showed little water solubility. The solubility of the nanocomposite containing 2% ZnO-HSP was decreased to 30% after 8 h, and the same value was reduced to 24% for the 6% ZnO-HSP nanocomposite. The % solubility value for the nanocomposite containing 4% ZnO-HSP was between the values of the other two nanocomposites (27%). The results showed that the ZnO-HSP nanoparticles added to PVA had reduced the hydrophilicity. The interaction of the OH and C=O groups in the structure of the ZnO-HSP nanoparticles with the OH groups of the PVA was more significant than the interaction with water; therefore, the solubility decreased.

3.12 Swelling Properties

The % swelling value results of PVA and nanocomposites are presented in Fig. 12b. The % equilibrium swelling values obtained are in the range of 2.025–1.790%. Among all tested samples, the highest % swelling value belonged to the pure PVA and the lowest to the nanocomposite containing 6% ZnO-HSP. A decrease in % swelling values was observed with the increase of the ZnO-HSP concentration in the nanocomposites. This showed that the ZnO-HSP in the structure had reduced the hygroscopicity of the nanocomposites. This can be attributed to the flexible network structure formed by intra- and inter-polymer chain reactions resulting from the hydrophilic hydroxyl side groups that the PVA carries [58]. The results showed that the ZnO-HSPs caused decreased water-holding capacity in the PVA, thus increasing the potential of the PVA-ZnO-HSP nanocomposites for use as food packaging materials. All these findings are compatible with the literature [46].

4 Conclusion

The PVA biopolymer has the potential for application as a carrier in active food packaging. However, its solubility in water and poor biological activity limit its use. In this study, the biological activity of the PVA was significantly improved by successfully loading the hesperidin-ZnO nanoparticles. Although the pure PVA showed no activity against *E. coli* and *S. aureus* bacteria, serious resistance against these pathogens was created because of the addition of the ZnO-HSP antimicrobial agent. The antioxidant properties of the PVA/ZnO-HSP nanocomposites reached a remarkable rate compared with those of vitamin C. The PVA-based nanocomposites showed no cytotoxic/proliferative effects against human G-361 melanoma cells. In addition, the ZnO-HSPs reduced the water solubility and water-holding capacity of pure PVA. The nanocomposites gained a significant thermal resistance compared to the pure PVA, and reduced softening temperatures were observed. The obtained results confirmed that PVA could be used as a reliable food packaging material with the addition of the ZnO-HSP nanoparticles.

Acknowledgements This study was supported by the Afyon Kocatepe University Scientific Research Projects Coordination Unit (Project Number 21-FENED-05).

Declarations

Conflict of interest The authors declare that they have no conflict of interest.

Ethical Approval Not applicable.

Informed Consent Not applicable.

Research Involving Human and Animal Participation Not applicable.

References

1. S. Elbasuney, A. Maraden, Novel thermoset nanocomposite intumescent coating based on hydroxyapatite nanoplates for fireproofing of steel structures. J. Inorg. Organomet. Polym. Mater. **30**(3), 820–830 (2020)
2. J. Bi. C. Tian, G.L. Zhang, H. Hao, H.M. Hou, Novel procyanidins-loaded chitosan-graft-polyvinyl alcohol film with sustained antibacterial activity for food packaging. Food Chem. **365**, 130534 (2021)
3. A. Kumar, Y.S. Negi, N.K. Bhardwaj, V. Choudhary, Synthesis and characterization of methylcellulose/PVA based porous composite. Carbohydr. Polym. **88**, 1364–1372 (2012)
4. T. Min, Z. Zhu, X. Sun, Z. Yuan, J. Zha, Y. Wen, Highly efficient antifogging and antibacterial Food Packaging Film fabricated by novel quaternary ammonium Chitosan Composite. Food Chem. **308**, 125682 (2019)
5. A.M. Youssef, S.M. EL-Sayed, H.S. EL-Sayed, H.H. Salama, A. Dufresne, Enhancement of egyptian soft white cheese shelf life using a novel chitosan/carboxymethyl cellulose/zinc oxide bionanocomposite film. Carbohydr. Polym. **151**, 9–19 (2016)
6. J. Jiang, J. Pi, J. Cai, The advancing of Zinc Oxide Nanoparticles for Biomedical Applications. Bioinorg. Chem. Appl. **5**, 1062562 (2018)
7. K.C. Barick, S. Nigam, D. Bahadur, Nanoscale assembly of mesoporous ZnO: a potential drug carrier. J. Mater. Chem. **20**, 6446–6452 (2010)
8. S.K. Shukla, S.R. Deshpande, S.K. Shukla, A. Tiwari, Fabrication of a tunable glucose biosensor based on zinc oxide/chitosan-graft-poly(vinyl alcohol) core-shell nanocomposite. Talanta **99**, 283–287 (2012)
9. H. Ghaffari, A. Tavakoli, A. Moradi, A. Tabarraei, F. Bokharaei-Salim, M. Zahmatkeshan, M. Farahmand, D. Javanmard, S.J. Kiani, M. Esghaei, V. Pirhajati-Mahabadi, S.H. Monavari, A. Ataei-Pirkooh, Inhibition of H1N1 influenza virus infection by zinc oxide nanoparticles: another emerging application of nanomedicine. Biomed. Sci. **26**, 70 (2019)
10. J. Suarez, M.D. Herrera, E. Marhuenda, Marhuenda, Invitro scavenger and antioxidant properties of hesperidin and neohesperidin dihydrochalcone. Phytomedicine **5**, 469–473 (1998)
11. N. Polat, O. Ciftci, A. Cetin, T. Yılmaz, Toxic effects of systemic cisplatin on rat eyes and the protective effect of hesperidin against this toxicity. Cutan. Ocul Toxicol. **35**, 1–7 (2016)
12. C. Wu, Y. Liu, Y. Yang, P. Zhang, W. Zhong, Y. Wang, Q. Wang, Y. Xu, M. Li, X. Li, M. Zheng, L. Chen, H. Li, Analysis of therapeutic targets for SARS-CoV-2 and discovery of potential drugs by computational methods. Acta Pharm. Sin B **10**, 766–788 (2020)
13. D. Das, B.C. Nath, P. Phukon, A. Kalita, S.K. Dolui, An investigation into the identification of potential inhibitors of SARS-CoV-2 main protease using molecular docking study. Colloids Surf. B **111**, 556–560 (2013)
14. R.S. Joshi, S.S. Jagdale, S.B. Bansode, S.S. Shankar, M.B. Tellis, V.K. Pandya, A. Chugh, A.P. Giri, M.J. Kulkarni, Discovery of potential multi-target-directed ligands by targeting host-specific SARS-CoV-2 structurally conserved main protease. J. Biomol. Struct. Dyn. **39**, 3099–3114 (2021)
15. X. Wang, C. Yang, Y. Sun, X. Sui, T. Zhu, Q. Wang, S. Wang, J. Yang, W. Yang, F. Liu, M. Zhang, Y. Wang, Y. Luo, A novel screening strategy of anti-SARS-CoV-2 drugs via blocking interaction between Spike RBD and ACE2. Environ. Int. **147**, 106361 (2021)
16. S. Mallakpour, M. Lormahdiabadi, Production of the ZnO-folic acid nanoparticles and poly(vinyl alcohol) nanocomposites: investigation of morphology, wettability, thermal, and antibacterial properties. J. Polym. Res. **27**, 259 (2020)
17. K.S. Hemalatha, K. Rukmani, N. Suriyamurthy, B.M. Nagabhushana, Synthesis, characterization and optical properties of hybrid PVA–ZnO nanocomposite: a composition dependent study. Mater. Res. Bull. **51**, 438–446 (2014)
18. S.A. Khan, S. Shahid, T. Mahmood, C.S. Lee, Contact lenses coated with hybrid multifunctional ternary nanocoatings (phytomolecule-coated ZnO nanoparticles: gallic acid: Tobramycin) for the treatment of bacterial and fungal keratitis. Acta Biomater. **128**, 262–276 (2021)
19. B. Lallo da Silva, B.L. Caetano, B.G. Chiari-Andréo, R.C.L.R. Pietro, L.A. Chiavacci, Increased antibacterial activity of ZnO nanoparticles: influence of size and surface modification. Colloids Surf. B Biointerfaces **177**, 440–447 (2019)
20. Q.U. Naqvi, A. Kanwal, S. Qaseem, M. Naeem, S.R. Ali, M. Shaffique, M. Maqbool, Size-dependent inhibition of bacterial growth by chemically engineered spherical ZnO nanoparticles. J. Biol. Phys. **45**, 147–159 (2019)
21. A. Masri, N.A. Khan, M. Zoqratt, Q. Ayub, A. Anwar, K. Rao, M.R. Shah, R. Siddiqui, Transcriptome analysis of Escherichia coli K1 after therapy with hesperidin conjugated with silver nanoparticles. BMC Mmicrobiol. **21**, 51 (2021)
22. G.H. Attia, D.A. Marrez, M.A. Mohammed, H.A. Albarqi, A.M. Ibrahim, M. Raey, Synergistic effect of Mandarin peels and hesperidin with Sodium Nitrite against some Food Pathogen Microbes. Molecules **26**, 3186 (2021)
23. Ö. Hazman, L. Aksoy, A. Büyükben, R. Kara, M. Kargıoğlu, Z.B. Kumral, İ Erol, Evaluation of antioxidant, cytotoxic, antibacterial effects and mineral levels of Verbascum lasianthum Boiss. Ex Bentham. An. Acad. Bras. Ciên **93**, e20210865 (2021)
24. Y. Huang, W. Zhou, J. Sun, G. Ou, N.S. Zhong, Z. Liu, Exploring the potential pharmacological mechanism of Hesperidin and Glucosyl Hesperidin against COVID-19 based on Bioinformatics analyses and antiviral assays. Am. J. Chin. Med. **50**, 351–369 (2022)
25. G.H. Attia, Y.S. Moemen, M. Youns, A.M. Ibrahim, R. Abdou, M.A. El, Raey, Antiviral zinc oxide nanoparticles mediated by hesperidin and in silico comparison study between antiviral phenolics as anti-SARS-CoV-2. Colloids Surf. B **203**, 111724 (2021)
26. F.J. Cheng, T.K. Huynh, C.S. Yang, D.W. Hu, Y.C. Shen, C.Y. Tu, Y.C. Wu, C.H. Tang, W.C. Huang, Y. Chen, C.Y. Ho, Hesperidin is a potential inhibitor against SARS-CoV-2 infection. Nutrients **13**, 2800 (2021)
27. L.A. Alshabanah, M. Hagar, L.A. Al-Mutabagani, G.M. Abozaid, S.M. Abdallah, H. Ahmed, A.H. Hassanin, N. Shehata, Biodegradable nanofibrous membranes for Medical and Personal Protection Applications: Manufacturing, Anti-COVID-19 and Anti-Multidrug resistant Bacteria evaluation. Materials **14**, 3862 (2021)
28. Ö Hazman, H. Evin, M.F. Bozkurt, İH. Ciğerci, Two faces of arbutin in hepatocellular carcinoma (HepG2) cells: anticarcinogenic effect in high concentration and protective effect against cisplatin toxicity through its antioxidant and anti-inflammatory activity in low concentration. Biologia **77**, 225–239 (2022)
29. G. Ersin, S. Çelik, S.S. Ulasli, A. Özyürek, Ö Hazman, S. Günay, M. Özdemir, M. Ünlü, Comparison of the anti-inflammatory Effects of Proanthocyanidin, Quercetin, and Damnacanthal on Benzo(a)pyrene exposed A549 alveolar cell line. Inflammation **39**(2), 744–751 (2016)

30. H.E. Kissinger, Reaction kinetics in differential thermal analysis. Anal. Chem. **29**, 1702–1706 (1957)
31. S. Shojaee-Aliabadi, H. Hosseini, M.A. Mohammadifar, A. Mohammadi, M. Ghasemlou, S.M. Ojagh, M.H. Seyede, K. Ramin, Characterization of antioxidant-antimicrobial -carrageenan films containing Satureja hortensis essential oil. Int. J. Biol. Macromol. **52**, 116–124 (2013)
32. X. Gong, C.Y. Tang, L. Pan, Z. Hao, C.P. Tsui, Characterization of poly(vinyl alcohol) (PVA)/ZnO nanocomposites prepared by a one-pot method. Compos. B Eng. **60**, 144–149 (2014)
33. J. Lee, K.J. Lee, J. Jang, Properties of nano-ZnO/poly(vinyl alcohol)/poly(ethylene oxide) composite thin films. Polym. Test. **27**, 360–367 (2008)
34. X.M. Sui, C.L. Shao, Y.C. Liu, White-light emission of polyvinyl alcohol/ZnO hybrid nanofibers prepared by electrospinning. Appl. Phys. Lett. **87**, 113115 (2005)
35. A. Chaturvedi, A.K. Bajpai, J. Bajpai, S.K. Singh, Evaluation of poly (vinyl alcohol) based cryogel–zinc oxide nanocomposites for possible applications as wound dressing materials. Mater. Sci. Eng. C **65**, 408–418 (2016)
36. D.M. Fernandes, A.A. Winkler Hechenleitner, S.M. Lima, L.H.C. Andrade, A.R.L. Caires, P. Gomez, Preparation, characterization, and photoluminescence study of PVA/ZnO nanocomposite films. Mater. Chem. Phys. **128**, 371–376 (2011)
37. S.B. Aziz, M.F.Z. Kadir,, M.H. Hamsan, H.J. Woo, M.A. Brza, Development of polymer blends based on PVA: POZ with low dielectric constant for microelectronic applications. Sci. Rep. **9**, 13163 (2019)
38. J. Selvi, V. Parthasarathy, S. Mahalakshmi, R. Anbarasan, M.O. Daramola, P. Senthil Kumar, Optical, electrical, mechanical, and thermal properties and non-isothermal decomposition behavior of poly(vinyl alcohol)-ZnO nanocomposites. Iran. Polym J **29**, 411–422 (2020)
39. S. Azizi, M. Ahmad, I. Nor, M. Hussein, F. Namvar, Cellulose Nanocrystals/ZnO as a Bifunctional reinforcing Nanocomposite for Poly(vinyl alcohol)/Chitosan Blend Films: fabrication, characterization and Properties. Int. J. Mol. Sci. **15**, 11040–11053 (2014)
40. J.W. Wang, C. Gao, Y.S. Zhang, Y.Z. Wan, Preparation and in vitro characterization of BC/PVA hydrogel composite for its potential use as artificial cornea biomaterial. Mater. Sci. Eng. C **30**, 214–218 (2010)
41. J. George, K.V. Ramana, A.S. Bawa, Siddaramaiah, bacterial cellulose nanocrystals exhibiting high thermal stability and their polymer nanocomposites. Int. J. Biol. Macromol. **48**, 50–57 (2011)
42. S.C. Liufu, H.N. Xiao, Y.P. Li, Thermal analysis and degradation mechanism of polyacrylate/ZnO nanocomposites. Polym. Degrad. Stab. **87**, 103–110 (2005)
43. J. Lee, D. Bhattacharyya, A.J. Easteal, J.B. Metson, Properties of nano-ZnO/poly(vinyl alcohol)/poly(ethylene oxide) composite thin films. Curr. Appl. Phys. **8**, 42–47 (2008)
44. I. Erol, Z. Gurler, A new methacrylate polymer functionalized with fluoroarylketone prepared by hydrothermal method and its nanocomposites with sio2: thermal, dielectric, and biocidal properties. Polym. Bull. (2022). https://doi.org/10.1007/s00289-022-04195-1
45. I. Erol, I.H. Cigerci, A. Ozkara, D. Akyıl, M. Aksu, Synthesis of moringa oleifera coated silver-containing nanocomposites of a new methacrylate polymer having pendant fluoroarylketone by hydrothermal technique and investigation of thermal, optical, dielectric and biological properties. J. Biomater. Sci. Polym. Ed. (2022). https://doi.org/10.1080/09205063.2022.2046986
46. A. Akbari, H. Jafari, G. Gohari, G. Kheiri, G.R. Mahdavinia, Fulvic acid-embedded poly (vinyl alcohol)–zinc oxide hydrogel nanocomposite: synthesis, characterization, swelling and release kinetic. Int. Nano Lett. **11**, 347–354 (2021)
47. V. Sharma, D. Anderson, A. Dhawan, Zinc oxide nanoparticles induce oxidative stress and genotoxicity in human liver cells (HepG2). J. Biomed. Nanotechnol **7**, 98–99 (2011)
48. P.K. Wilmsen, D.S. Spada, M. Salvador, Antioxidant activity of the flavonoid hesperidin in chemical and biological systems. J. Agric. Food Chem. **53**, 4757–4761 (2005)
49. G.M. Sulaiman, H.M. Waheeb, M.S.S.H. Jabir, Y.H. Hazaal, Y. Dewir, Naidoo, Hesperidin Loaded on Gold Nanoparticles as a drug delivery system for a successful Biocompatible, Anti-Cancer, anti-inflammatory and phagocytosis inducer Model. Sci. Rep. **10**, 9362 (2020)
50. S.K. Evstropiev, K.V. Dukelskii, A.V. Karavaeva, V.N. Vasilyev, E.V. Kolobkova, N.V. Nikonorov, K.S. Evstropyev, Transparent bactericidal ZnO nanocoatings. J. Mater. Sci. Mater. Med. **28**, 102 (2017)
51. S. Alarifi, D. Ali, S. Alkahtani, A. Verma, M. Ahamed, M. Ahmed, H.A. Alhadlaq, Induction of oxidative stress, DNA damage, and apoptosis in a malignant human skin melanoma cell line after exposure to zinc oxide nanoparticles. Int. J. Nanomedicine **8**, 983–993 (2013)
52. Y. Wang, H. Yu, J. Zhang, J. Gao, X. Ge, G.Lou, Hesperidin inhibits HeLa cell proliferation through apoptosis mediated by endoplasmic reticulum stress pathways and cell cycle arrest. BMC Cancer **15**, 682 (2015)
53. N. Poier, J. Hochstöger, S. Hackenberg, A. Scherzad, M. Bregenzer, D. Schopper, N. Kleinsasser, Effects of Zinc Oxide Nanoparticles in HUVEC: Cyto- and genotoxicity and functional impairment after long-term and repetitive exposure in vitro. Int. J. Nanomedicine **15**, 4441–4452 (2020)
54. K.M. Amin, A.M. Partila, H.A. Abd El Rehim, N.M. Deghiedy, Antimicrobial ZnO nanoparticle–doped polyvinyl alcohol/pluronic blends as active food packaging films. Particle Particle Syst. Charact **37**, 2000006 (2020)
55. Y. Kaneo, S. Hashihama, A. Kakinoki, T. Tanaka, T. Nakano, Y. Ikeda, Pharmacokinetics and Biodisposition of Poly(vinyl alcohol) in rats and mice. Drug Metab. Pharmacokinet. **20**, 435–442 (2005)
56. G. Rivera-Hernández, M. Antunes-Ricardo, P. Martínez-Morales, M.L. Sánchez, Polyvinyl alcohol based-drug delivery systems for cancer treatment. Int. J. Pharm. **600**, 120478 (2021)
57. R. Jangde, G.O. Elhassan, S. Khute, D. Singh, M. Singh, R.K. Sahu, J. Khan, Hesperidin-loaded lipid polymer hybrid nanoparticles for topical delivery of bioactive drugs. Pharmaceuticals **15**, 211 (2022)
58. H. He, R. Cai, Y.Wang, et al., Preparation and characterization of silk sericin/PVA blend film with silver nanoparticles for potential antimicrobial application. Int. J. Biol. Macromol. **104**, 457–464 (2017)

Publisher's Note Springer Nature remains neutral with regard to jurisdictional claims in published maps and institutional affiliations.

Springer Nature or its licensor (e.g. a society or other partner) holds exclusive rights to this article under a publishing agreement with the author(s) or other rightsholder(s); author self-archiving of the accepted manuscript version of this article is solely governed by the terms of such publishing agreement and applicable law.